Research Article

The Facile Synthesis of Novel ZnO Nanostructure for Galactose Biosensor Application

Phuong Ha La Phan,[1] Quang Trung Tran [ID],[1] Duc Anh Dinh,[2] Ko Kang Bok,[2,3] Chang-Hee Hong,[3] and Tran Viet Cuong [ID][2,3]

[1]*Department of Solid State Physics, University of Science, Vietnam National University-Ho Chi Minh City (VNU-HCM), 227 Nguyen Van Cu, Ward 4, District 5, Ho Chi Minh City, Vietnam*
[2]*NTT Hi-Tech Institute, Nguyen Tat Thanh University, 298-300 A Nguyen Tat Thanh Street, Ho Chi Minh City, Vietnam*
[3]*LED Agri-Bio Fusion Technology Research Center, Chonbuk National University, Jeonju 561-853, Republic of Korea*

Correspondence should be addressed to Quang Trung Tran; tqtrung@hcmus.edu.vn and Tran Viet Cuong; tvcuong@ntt.edu.vn
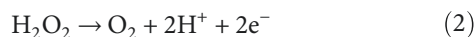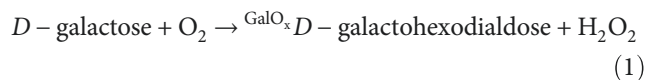
We introduce a novel structure of ZnO nanorods (NRs) grown on ZnO NRs (ZnO NRs/NRs) via a facile, low-cost, and environmentally friendly synthesis for galactose biosensor application. The galactose oxidase enzyme ($GalO_x$) is immobilized on the ZnO NR/NR surface to form the novel electrode structure ($GalO_x$|ZnO NRs/NRs). The $GalO_x$|ZnO NR/NR electrode has a linear detection range of current density from $11.30\,\mu A/mm^2$ to $18.16\,\mu A/mm^2$ over a galactose concentration range from 40 mM to 230 mM, indicating the increment of electrode sensitivity up to 60.7%. The ZnO NR/NR morphology with a high surface area to volume ratio has a great contribution to the electrochemical performance of galactose biosensor. Our results propose a straightforward approach to fabricate architecturally ZnO-based nanostructure for biosensor application.

1. Introduction

Galactose (Gal), a common monosaccharide, is an important energy resource in living organisms [1]. Gal in the human body can be converted into glucose, which is the primary fuel for cellular energy production. The metabolism of Gal is based on the hydrolysis of lactose, which involves the significant contribution of various types of enzymes such as galactokinase, galactose-1-phosphate uridylic transferase, beta-galactoside, and galactose-6-phosphate epimerase [2]. However, the metabolism of Gal can cause the detrimental effect to the human body, so-called galactosemia, when the amount of one of the enzymes is insufficient [3]. The galactosemia is an inherited disorder that affects how our body processes Gal, and the symptoms of galactosemia result from an inability to use Gal to produce energy [4]. For instance, a high level of Gal in infant bodies (>1.1 mM) may develop cataracts, liver diseases, and kidney problems [5]. Even with

medical treatment, children may suffer from learning disabilities, and females with galactosemia may have problems with their ovaries [5, 6]. In the most serious case, the build-up of Gal can be very dangerous to the brain, leading to death [7]. Therefore, the quantitative determination and control of the Gal level in the human body, food, or dairy products are extremely important. So far, the most common method for the Gal analysis is the enzyme-based techniques using two types of enzymes: galactose oxidase ($GalO_x$) or galactose dehydrogenase (GADH), in association with spectrophotometric, polarimetric, and fluorometric detection of enzymatic products [8, 9]. The GADH technique has been developed and commercialized; however, it is still expensive, time-consuming, and inconvenient (requires skilled personnel to operate them) [8–10]. Thus, electrochemical measurements, especially in conjunction with the use of amperometric biosensors based on $GalO_x$, are becoming more attractive for Gal analysis [11]. Such biosensors

utilize the capability of GalO$_x$ to catalyze Gal, as described by the following equations:

$$D - galactose + O_2 \rightarrow {}^{GalO_x} D - galactohexodialdose + H_2O_2 \tag{1}$$

$$H_2O_2 \rightarrow O_2 + 2H^+ + 2e^- \tag{2}$$

The electrochemical monitoring of the enzymatically produced H$_2$O$_2$ provides the analytical response. In fact, the electron transfer of the reaction of H$_2$O$_2$ can be detected easily even at low potentials, providing the signal of current in electrochemical measurement [11]. These anodic and cathodic currents are directly proportional to the amount of Gal [12, 13]. These aspects of GalO$_x$-based electrochemical biosensors would allow for the development of rapid, highly selective, sensitive, and low-cost analytical devices. The key feature of such biosensors is properties of electrode materials which allow the effective immobilization of the GalO$_x$ enzyme, one of the best catalytic agents for Gal [14]. In recent years, many efforts have been focused on the development of metallic nanoparticle- (NP-) based Gal biosensor, e.g., gold NPs, due to their good conductivity, electrocatalytic ability, biocompatibility, and availability of many active sites [15–17]. However, these NPs are very easy to be aggregated, inducing the deterioration of their outstanding properties and instability of GalO$_x$ immobilization [18, 19]. Another choice of electrode material is the use of cross-linking polymers, forming the three-dimensional network to entrap GalO$_x$ [20–22]. The use of synthetic polymers such as polyurethane, polyacrylamide, polyvinylchloride, polyvinyl alcohol, and polyvinyl formal (PVF) provides several advantages such as chemical resistance, high mechanical strength, and the feasible combination with buffer components [23, 24]. However, most of the disadvantages of these polymers are their poor conductivity, hindering the direct electron transfer (DET) between an enzyme and electrode. The disadvantages of NPs and polymers turn out that the proper materials for Gal biosensor must possess the proper physical/chemical properties and structure to guarantee not only the enzyme immobilization but also the DET process. In this context, ZnO has been recognized as a promising electrode material for Gal biosensor due to its interesting properties such as good chemical stability, good electron transport, nontoxic, high biological compatibility, and high isoelectric point (IP 9.5) [25–27]. In terms of material design, ZnO can be available in a variety of nanostructures such as nanowires, nanorods, and nanotubes which can be grown at the low temperature via the solution method [28]. Among these nanostructures, ZnO nanorod (NR) has shown numerous applications in the fields of bioelectronics because its high surface area to volume ratios allow great combination with immobilized enzymes [14, 29, 30]. Moreover, ZnO can maintain the activity of the enzyme due to the high biocompatibility and enhance the DET between the enzyme's active sites and the electrode. Also, the high IP of ZnO (9.5) makes it a good matrix to immobilize low isoelectric point enzymes, e.g., GalO$_x$ (4.61), by electrostatic interactions with high binding stability [31, 32].

Herein, we fabricate a novel nanostructure of ZnO NRs grown on ZnO NRs (ZnO NRs/NRs) using the solution method. The produced nanostructure demonstrates a significant increase in surface area to volume ratio with respect to that of ZnO NRs only, for Gal biosensor. Furthermore, GalO$_x$ is successfully immobilized in the ZnO NRs/NRs by using glutaraldehyde as a cross-linker. The effect of the morphologies of the ZnO nanocrystals on the GalO$_x$ immobilization applied in Gal biosensor is systematically studied. Our result is opening a new strategy to synthesize the novel ZnO nanostructure based on a facile, low-cost, and eco-friendly method for Gal biosensor application.

2. Experimental

2.1. Reagents and Materials. For synthesis of ZnO NRs, zinc acetate dihydrate Zn(CH$_3$COO)$_2$·2H$_2$O, ethanol C$_2$H$_5$OH, and monoethanolamine NH$_2$CH$_2$CH$_2$OH are purchased from Merck, Germany. Acetone C$_3$H$_6$O is obtained from QREC, Malaysia. The phosphate buffered saline (pH = 7.4) is purchased from HiMedia, India. Glutaraldehyde C$_5$H$_8$O$_2$ is purchased from Merck, and galactose oxidase (lyophilizes powder ≥ 3000 units/g solid) was from Sigma-Aldrich.

2.2. The Growth of ZnO NRs and ZnO NRs/NRs on FTO Substrate. Reagent grade (RG) zinc acetate dihydrate and monoethanolamine (MEA) were first dissolved in an ethanol solvent with a Zn^{2+} concentration of 0.75 M to form a seed solution. This solution was magnetically stirred at room temperature for 2 hours. Fluorine doped tin oxide (FTO) substrate was coated with the seed solution by using a spin coating and then annealed at 500°C to form a ZnO seed layer. The size (area) of the FTO substrate is 1.2 cm^2.

The ZnO NRs and ZnO NRs/NRs were fabricated from seed ZnO-coated FTO substrate. The ZnO NRs were used as a reference to evaluate the effect of ZnO NP/NR morphology on the performance of Gal biosensor. In detail, precursor zinc nitrate dehydrates (Zn(NO$_3$)$_2$·2H$_2$O) and hexamethylenetetramine (HMTA, C$_6$H$_{12}$N$_4$) were dissolved in an aqueous solution with a Zn^{2+} concentration of 0.02 M. This solution was stirred at room temperature for 2 hours. After that, the prepared ZnO seed layer on FTO substrate was dipped in that solution and kept in an oven at 80°C for 2 hours to form ZnO NRs. To synthesize ZnO NRs/NRs, the FTO-coated ZnO seed layer was dipped in above solution for 5 hours at 80°C to form large ZnO NRs; the small ZnO NRs were subsequently grown at 80°C for 2 hours. Finally, products are rinsed with water and dried in an argon stream.

2.3. The Immobilization of the Galactose Oxidase Enzyme on ZnO Nanostructures. The 2.5% glutaraldehyde (GA) in 0.1 mM phosphate buffer solution (PBS) and GalO$_x$ solution in PBS having a concentration of 2 mg/mL of enzyme are mixed in one bottle, then ZnO substrate is dipped into it in 3.5 hours at room temperature to examine the saturation
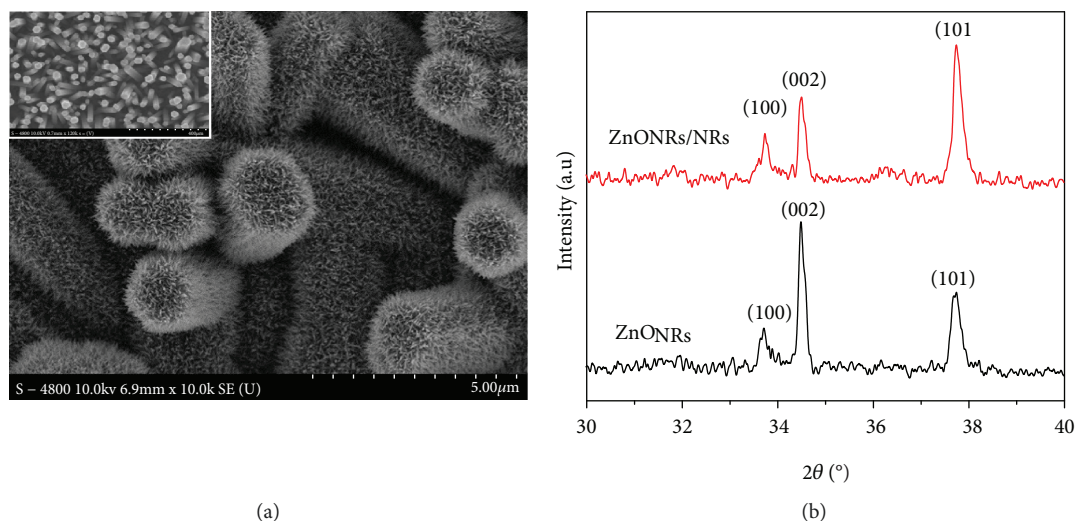
(a)

(b)

FIGURE 1: (a) Scanning electron microscope and (b) X-ray diffraction patterns of RD of ZnO NRs and ZnO NRs/NRs.

of the ZnO surface with the $GalO_x$ enzyme immobilized ZnO electrode ($GalO_x$|ZnO).

2.4. Characterization. The ZnO NR samples were characterized by X-ray diffraction spectrometer (XRD) D8 Bruker with Cu Kα radiation source ($\lambda = 1.5417$ Å), 2θ range 30–40°, 0.03° step size, and scanning speed = 12°/min. The surface morphology of ZnO NRs and ZnO NR/NR samples was investigated by FE-SEM S4800–Hitachi at the voltage of 10 kV.

The optical absorption spectra (OAS) of $GalO_x$ enzyme solution after the immobilization on ZnO NRs were measured by UV-Vis spectroscopy U2910, Hitachi, Japan ($\lambda = 450 – 700$ nm).

The FTIR spectroscopy of ZnO NRs and ZnO NR/NR samples after and before $GalO_x$ enzyme immobilization was carried out by an FTIR spectrophotometer JASCO-4700, Japan (wavenumber range 500–3500 cm^{-1}).

The electrochemical properties of the proposed Gal biosensor based on the $GalO_x$ immobilized ZnO NRs and ZnO NR/NR electrode in Gal solution (200 mM) were measured by the cyclic voltammetry (CV) method with the MPG-2 analyzer (Bio-Logic), using $GalO_x$|ZnO NRs and $GalO_x$|ZnO NRs/NRs as a working electrode, a platinum plate as the counter electrode, and an Ag/AgCl electrode as the reference one. Then the measurement was carried out at a scan rate of 100 mV/s with the potential range from -0.5 V to 1.0 V.

3. Results and Discussion

3.1. Structure and Morphology of ZnO Nanostructures. In this work, the ZnO NR/NR structure is grown by means of the solution method which has the advantages of simplicity, low-cost, and environment-friendliness. The surface morphology of ZnO and ZnO NRs/NRs is examined by SEM. Figure 1(a) depicts SEM micrograph of ZnO NRs/NRs; the inset showing the morphology of ZnO NRs only. The SEM images of ZnO NRs show the hexagonal structure of these NRs with the higher vertical alignment on ZnO

seed-coated FTO substrate, and the average diameter of NRs is about 45 nm. The well-aligned ZnO NR arrays could be attributed to the effective growth of ZnO seeds via the solution method. The one-dimensional (1D) structure of ZnO NRs supplies good orientation and a large surface area which is favorable for enzyme immobilization. Besides, the SEM image of the ZnO NRs/NRs describes a novel morphology of the small ZnO NRs grown on the large ZnO NRs (the average diameter of large ZnO NRs is 800 nm). This morphology provides the larger surface area than ZnO NRs only (see the inset), allowing the higher quantity of enzyme immobilized on the ZnO NR/NR surface with respect to ZnO NRs. The structure and lattice parameters of ZnO NRs and ZnO NRs/NRs are analyzed by X-ray diffraction (XRD). As shown in Figure 1(b), the XRD patterns of ZnO NRs and ZnO NRs/NRs show three typical peaks (100), (002), and (101) are located at $2\theta = 33.5°$, 34.5°, and 37.7° (JCPDF card no 36-1451), respectively, suggesting the hexagonal wurtzite lattice of ZnO NRs [33, 34]. The typical (002) peaks appear at 34.5°, presenting the preferential orientation of NRs along the c–axis. In the case of ZnO NRs, the intensities of other peaks such as (100) and (101) are comparatively lower than that of (002) peaks, implying the fact that the highly oriented along c–axis of ZnO NRs, perpendicular to the plane of the FTO substrate. However, the XRD pattern of ZnO NRs/NRs shows the significant increase in intensities of (100) and (101) peaks with respect to that of the (002) peak. It is because the growth of small ZnO NRs on the surface of large ZnO NRs causes the rise of different orientations, e.g, (100) and (101) other than preferential (002) orientation. The XRD result of ZnO NRs and ZnO NRs/NRs is in agreement with the morphological characterization in SEM images, as shown in Figure 1(a).

3.2. The Activity of Working Electrodes Based on Different Morphologies of ZnO. The FT-IR spectroscopy was used to study the enzyme immobilization on the ZnO NR surface. Figure 2 shows the FT-IR spectra of ZnO NRs và ZnO
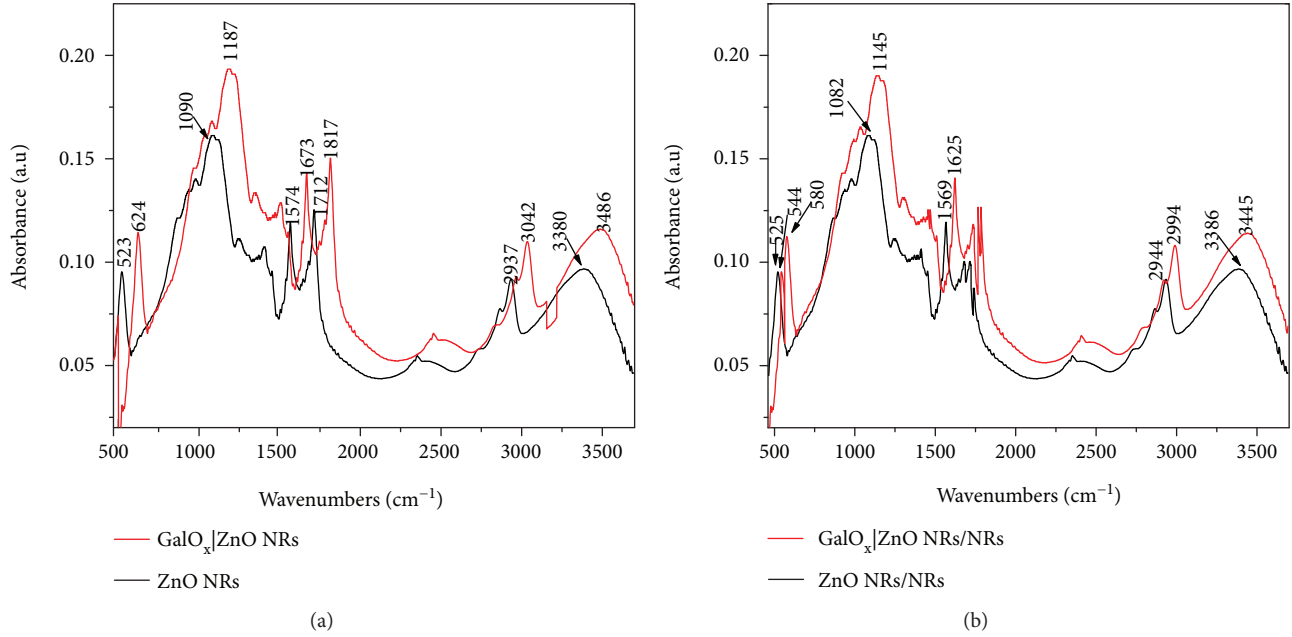
(a)

(b)

FIGURE 2: FT-IR spectra of (a) ZnO NRs and (b) ZnO NRs/NRs after and before $GalO_x$ enzyme immobilization.

NRs/NRs before and after successful $GalO_x$ enzyme immobilization. Before $GalO_x$ immobilization, the peaks at ~523-525 cm^{-1} correlated to stretching modes of Zn-O [35], whereas the peaks at ~3386–3380 cm^{-1} and 1569 cm^{-1} corresponding to O-H hydroxyl stretching vibration of absorbed water molecules on the surface of the ZnO NRs are clearly observed in both cases of ZnO NRs and ZnO NRs/NRs [14, 36]. After the $GalO_x$ immobilization, the peaks at ~525, 1082, 1569, 2944, and 3386 cm^{-1} are shifted to the right-hand side, indicating the interaction between the $GalO_x$ with the surface of the ZnO NRs. The presence of different peaks in the spectra might be because of impurity in samples [14].

The amount of the $GalO_x$ enzyme immobilized on the ZnO surface is calculated by the Bradford method [35, 36]. The principle of this method relies on the change of maximum absorption wavelength of the Coomassie Brilliant Blue (CBB) reagent in the presence of different bovine serum albumin (BSA) protein concentrations. It is necessary to build the calibration curve before calculating the concentration of $GalO_x$. To realize this, the different concentrations of BAS protein are added into CBB to form the homogeneous solutions (six samples). The optical density (OD) values of these solutions are measured at the wavelength of 595 nm. It has been reported that without the albumin enzyme, the maximum absorption peak can be obtained at the wavelength of 465 nm [37]. However, the maximum absorption wavelength changes to 595 nm when adding albumin to this solution [37]. Therefore, the OD of enzyme solution is measured at 595 nm wavelength, and this OD value relates to BSA content in solution. By Bradford method, the calibration curve is plotted based on the linear relation of BSA concentrations and OD of enzyme solutions, as shown in Figure 3. Importantly, the
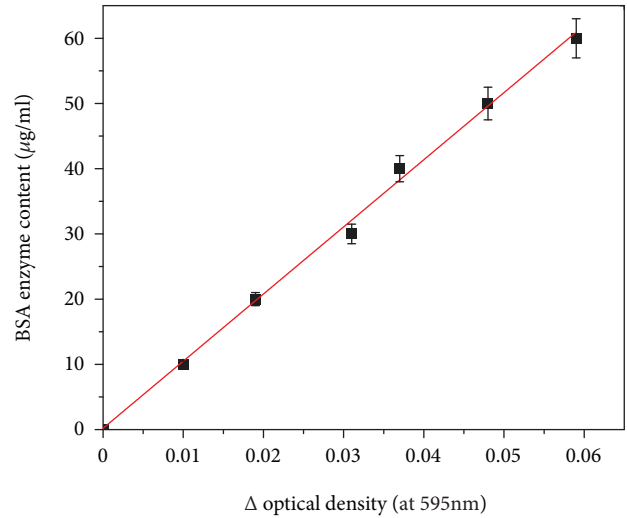

FIGURE 3: The calibration curve of the Bradford method.

calibration curve delivers the standard equation for the calculation of the $GalO_x$ concentration, as follows:

$$y = 1030.1x - 0.0195, \qquad (3)$$

where y is the OD value of the enzyme at 595 nm and x is the concentration of the enzyme.

Equation (3) expresses the regression line with the regression coefficient of 1030.1 and the intercept of -0.0195. Thus, the limit of detection (LOD) [38, 39] could be estimated as the following:

$$LOD = 3.3 \left(\frac{SE\sqrt{n}}{Regression\ coefficient} \right) \qquad (4)$$
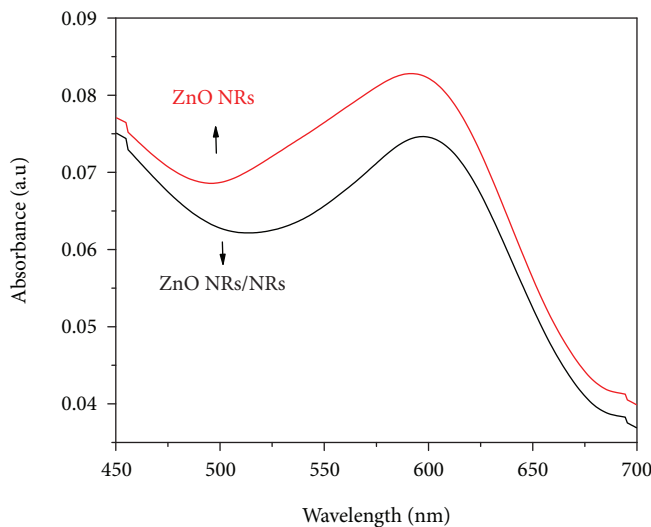
FIGURE 4: Optical absorption spectra of GalO$_x$ enzyme solution after the immobilization on ZnO NRs and ZnO NR/NR surfaces.

TABLE 1: Optical density values and the efficiency of the GalO$_x$ enzyme immobilization on ZnO NRs and ZnO NR/NR surfaces.

Sample	GalO$_x$|ZnO NRs	GalO$_x$|ZnO NRs/NRs
OD value	0.083	0.075
ΔOD	0.022	0.014
Enzyme concentration (find out from Bradford standard graph) (μg)	23.1	14.5
Enzyme content after the immobilization (μg)	1.155	725
Immobilized enzyme content (μg)	845	1.275
$H\%$	42.25	63.75

where LOD is the limit of detection, SE is the standard error of intercept which can be calculated to be 0.889, n is the number of measurements, and the value of regression coefficient is 1030.1. Therefore, the value of LOD of the calibration cure (Figure 3) is calculated as $5.47E^{-5}$.

In this study, the BSA protein is replaced by the GalO$_x$ enzyme. The GalO$_x$ contents immobilized on ZnO NRs and ZnO NRs/NRs are calculated from the OD values of GalO$_x$ enzyme solutions after 3.5 hours of immobilization. Moreover, the efficiency of the immobilization ($H\%$) can be found out based on the calibration curve:

$$H\% = \frac{C_0 - C_i}{C_0} \cdot 100\%, \tag{5}$$

where C_0 is the concentration of the enzyme at the beginning and C_i is the concentration of the enzyme after immobilization.

The OAS spectra of these enzyme solutions in both cases of ZnO NRs and ZnO NRs/NRs after the immobilization are acquired in the 450 nm to 700 nm wavelength range to obtain the OD values. As shown in Figure 4, the absorption peaks at ~525 nm associated with the OD values of enzyme solutions of 0.0745 and 0.827 for ZnO NRs and ZnO NRs/NRs, respectively. The efficiency of the GalO$_x$ immobilization on the ZnO NR surface is 42.3%, and it increases to 63.8% when GalO$_x$ is immobilized on ZnO

NR/NR surface. It is clearly demonstrated that the amount of the GalO$_x$ enzyme immobilized on the ZnO NR/NR surface increases because of the high surface to volume ratio of the ZnO NR/NR structure. The ZnO NR/NR structure can be featured on a three-dimensional structure, providing a high surface area for the larger enzyme immobilization with respect to the case of ZnO NRs only [11, 40]. The OD values and immobilization efficiencies of the GalO$_x$ enzyme solutions after the immobilization on ZnO NRs and ZnO NRs/NRs were summarized in Table 1.

To examine the catalytic activity of ZnO-based immobilized electrodes, we performed cyclic voltammetry measurement. All experiments are carried out with GalO$_x$ immobilized ZnO NRs (GalO$_x$|ZnO) and GalO$_x$ immobilized ZnO NR/NR (GalO$_x$|ZnO NRs/NRs) electrodes at a scan rate of 100 mV/s with the potential range from -0.5 V to 1.0 V. As shown in Figure 5, the cyclic voltammograms (CV) of GalO$_x$|ZnO NRs express the oxidation peak at 0.3 V, and the current density is observed about 0.12 μA/mm^2. On the other hand, in the case of the GalO$_x$|ZnO NR/NR electrode, this peak appears at 0.25 V with the enhanced value of current density 0.18 μA/mm^2 with respect to that of the GalO$_x$|ZnO NR electrode. The presence of these two oxidation peaks indicates the oxidation of Gal with the GalO$_x$ catalyst assist, which has been well explained by equations (1) and (2) [13]. Moreover, the potential difference between these two peaks (0.3 V
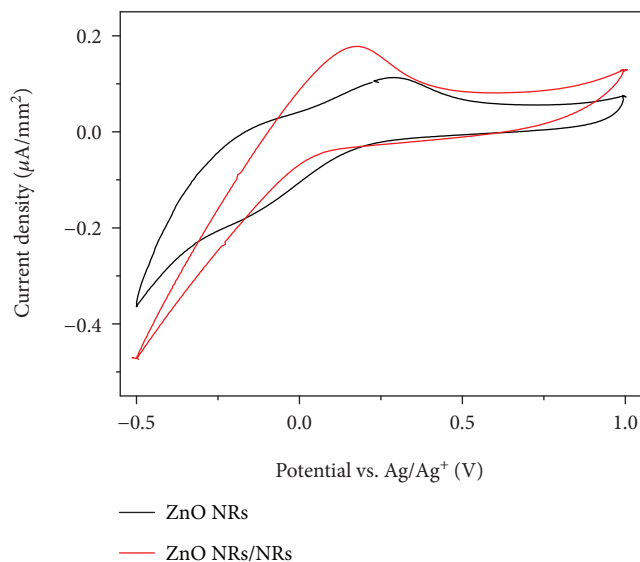
FIGURE 5: The cyclic voltammograms of GalO$_x$|ZnO NRs and GalO$_x$|ZnO NR/NR electrodes in 200 mM galactose solution at a scan rate of 100 mV/s.

FIGURE 6: The plots of current density vs. the Gal concentration of GalO$_x$|ZnO NRs/NRs and GalO$_x$|ZnO NRs.

and 0.25 V) may be since the different contact resistances caused the difference of interface contact between GalO$_x$ and ZnO surfaces. Importantly, the higher current density of the GalO$_x$|ZnO NR/NR electrode ($0.18 \mu A/mm^2$) with respect to the GalO$_x$|ZnO NR ($0.12 \mu A/mm^2$) one indicates that more oxidation reactions are taking place on the surface of the GalO$_x$|ZnO NR/NR electrode than that of GalO$_x$|ZnO NRs. This result confirms the novel morphology of ZnO NRs/NRs (see SEM image in Figure 1(a)), providing the high surface to volume ratio to increase the amount of the GalO$_x$ enzyme immobilized on the ZnO surface (as calculated in Table 1). The high concentration of GalO$_x$ promotes the oxidation of Gal by its catalytic capability, promoting the electron transfer process (see equations (1) and (2)) of reaction which causes the enhancement of the peak current density.

The various cyclic voltammetry measurements of GalO$_x$|ZnO NRs and GalO$_x$|ZnO NR electrodes in different concentrations of Gal solution, ranging from 40 mM to 230 mM, are carried out to evaluate the performance of these biosensors. The current densities delivered from the oxidation peaks in the CV results of GalO$_x$|ZnO NRs and GalO$_x$|ZnO NR/NR electrodes exhibit the linear correlation with the Gal concentrations, as illustrated in Figure 6. In the case of the GalO$_x$|ZnO NR electrode, the average current density linearly increases with the increasing of Gal concentration. This linear correlation is expressed by equation $y = 0.0142x + 9.3511$, as depicted in the black line in Figure 6. On the other hand, this linear correlation, see the red line in Figure 6, is associated with equation $y = 0.0369x + 10.063$ in the case of GalO$_x$|ZnO NRs/NRs. The values of regression coefficients are calculated to be 0.0139 and 0.0364 for GalO$_x$|ZnO NRs and GalO$_x$|ZnO NRs/NRs, respectively. Besides, according to equation (4), the LODs are calculated to be 105.62 mM and 54.742 mM for GalO$_x$|ZnO NRs and GalO$_x$|ZnO NRs/NRs, respectively. These results imply the better sensitivity of the GalO$_x$|ZnO
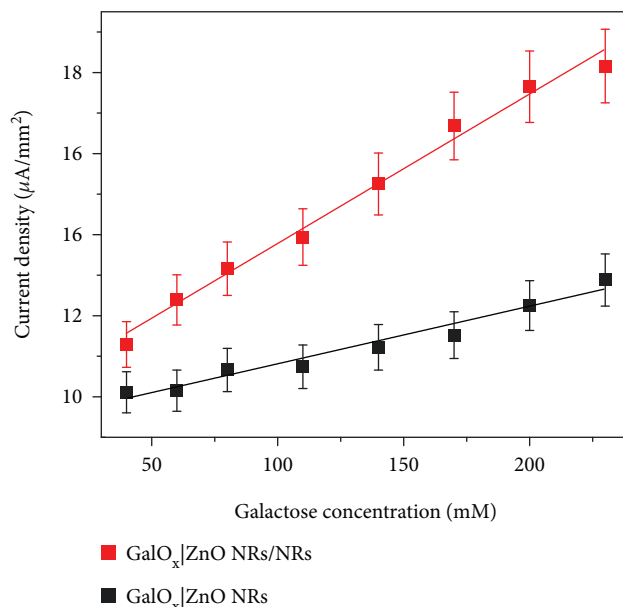
NR/NR electrode with respect to the GalO$_x$|ZnO NR one at the elevated concentration of Gal.

Also, with the increased concentration of GalO$_x$ from 40 mM to 230 mM, the current density of the GalO$_x$|ZnO NR electrode increases from $10.11 \mu A/mm^2$ to $12.88 \mu A/mm^2$, implying the increase of 27.40%. Meanwhile, the current density of the GalO$_x$|ZnO NR/NR electrode increases from $11.30 \mu A/mm^2$ to $18.16 \mu A/mm^2$, corresponding to the increment of 60.7%. This demonstrates that the sensitivity of the GalO$_x$|ZnO NR/NR electrode is superior to that of the GalO$_x$|ZnO NR one. These results come from the novel structure of ZnO NRs/NRs with a high surface area, providing the increase in the amount of GalO$_x$ enzyme immobilization with respect to the ZnO NR structure.

4. Conclusion

A novel nanostructure of ZnO NRs/NRs has been successfully synthesized via the solution method. This structure enables the excellent GalO$_x$ immobilization since its special morphology provides a high surface area to volume ratio, therefore enhancing the performance of Gal biosensor. Remarkably, the electrochemical response acquired from CV analysis shows that the current density of the GalO$_x$|ZnO NR/NR ($0.18 \mu A/mm^2$) electrode is higher than that of the GalO$_x$|ZnO NR electrode ($0.12 \mu A/mm^2$). Moreover, as the concentration of Gal solution increases from 40 mM to 230 mM, the sensitivity of the GalO$_x$|ZnO NR/NR electrode increases 60.7%, which is much higher than that of the GalO$_x$|ZnO NR one (27.4%). Thus, the novel structure of ZnO NRs/NRs is opening a promising research direction in material synthesis via the facile, low-cost, and environmentally friendly method, for high-performance biosensors.

Data Availability

(1) The data supporting the findings (figures and table) of this study are available within the article. (2) The data that support the findings of this study (figures and table) are available from the corresponding author (Dr. Tran Viet Cuong) upon reasonable request.

Conflicts of Interest

The authors declare that they have no conflicts of interest.

Acknowledgments

References

[1] P. B. Acosta and K. C. Gross, "Hidden sources of galactose in the environment," *European Journal of Pediatrics*, vol. 154, no. S2, pp. S87–S92, 1995.

[2] A. I. Coelho, G. T. Berry, and M. E. Rubio-Gozalbo, "Galactose metabolism and health," *Current Opinion in Clinical Nutrition and Metabolic Care*, vol. 18, no. 4, pp. 422–427, 2015.

[3] G. T. Berry, "Disorders of galactose metabolism," in *Rosenberg's Molecular and Genetic Basis of Neurological and Psychiatric Disease (Fifth Edition)*, pp. 615–626, Inborn Metabolic Diseases, Springer, 2015.

[4] A. M. Bosch, "Classic galactosemia: dietary dilemmas," *Journal of Inherited Metabolic Disease*, vol. 34, no. 2, pp. 257–260, 2011.

[5] S. S. Gropper, K. C. Gross, and S. J. Olds, "Galactose content of selected fruit and vegetable baby foods: implications for infants on galactose-restricted diets," *Journal of the American Dietetic Association*, vol. 93, no. 3, pp. 328–330, 1993.

[6] S. G. Kahler and M. C. Fahey, "Metabolic disorders and mental retardation," *American Journal of Medical Genetics*, vol. 117C, no. 1, pp. 31–41, 2003.

[7] G. T. Berry, "Galactosemia and amenorrhea in the adolescent," *Annals of the New York Academy of Sciences*, vol. 1135, no. 1, pp. 112–117, 2008.

[8] J. Tkáč, P. Gemeiner, and E. Šturdík, "Rapid and sensitive galactose oxidase-peroxidase biosensor for galactose detection with prolonged stability," *Biotechnology Techniques*, vol. 13, no. 12, pp. 931–936, 1999.

[9] P. Kanyong, R. M. Pemberton, S. K. Jackson, and J. P. Hart, "Development of an amperometric screen-printed galactose biosensor for serum analysis," *Analytical Biochemistry*, vol. 435, no. 2, pp. 114–119, 2013.

[10] P. Kanyong, G. Hughes, R. M. Pemberton, S. K. Jackson, and J. P. Hart, "Amperometric screen-printed galactose biosensor for cell toxicity applications," *Analytical Letters*, vol. 49, no. 2, pp. 236–244, 2016.

[11] P. Kanyong, F. D. Krampa, Y. Aniweh, and G. A. Awandare, "Enzyme-based amperometric galactose biosensors: a review," *Microchimica Acta*, vol. 184, no. 10, pp. 3663–3671, 2017.

[12] W. Shi and Z. Ma, "Amperometric glucose biosensor based on a triangular silver nanoprisms/chitosan composite film as immobilization matrix," *Biosensors & Bioelectronics*, vol. 26, no. 3, pp. 1098–1103, 2010.

[13] M. Sharma and M. Sharma, "Amperometric galactose biosensor based on silver nanoparticles/carboxylated multiwalled carbon nanotubes/polyaninine composite film," *International Journal of Recent Scientific Research*, vol. 8, no. 8, pp. 18976–18983, 2017.

[14] K. Khun, Z. H. Ibupoto, O. Nur, and M. Willander, "Development of galactose biosensor based on functionalized ZnO nanorods with galactose oxidase," *Journal of Sensors*, vol. 2012, Article ID 696247, 7 pages, 2012.

[15] J. M. Pingarrón, P. Yáñez-Sedeño, and A. González-Cortés, "Gold nanoparticle-based electrochemical biosensors," *Electrochimica Acta*, vol. 53, no. 19, pp. 5848–5866, 2008.

[16] M. Vidotti, R. F. Carvalhal, R. K. Mendes, D. C. M. Ferreira, and L. T. Kubota, "Biosensors based on gold nanostructures," *Journal of the Brazilian Chemical Society*, vol. 22, no. 1, pp. 3–20, 2011.

[17] Y. Li, H. J. Schluesener, and S. Xu, "Gold nanoparticle-based biosensors," *Gold Bulletin*, vol. 43, no. 1, pp. 29–41, 2010.

[18] Y. Zhang, Y. Liu, J. He, P. Pang, Y. Gao, and Q. Hu, "Electrochemical behavior of caffeic acid assayed with gold nanoparticles/graphene nanosheets modified glassy carbon electrode," *Electroanalysis*, vol. 25, no. 5, pp. 1230–1236, 2013.

[19] F. Zhang and M. P. Srinivasan, "Multilayered gold-nanoparticle/polyimide composite thin film through layer-by-layer assembly," *Langmuir*, vol. 23, no. 20, pp. 10102–10108, 2007.

[20] S. K. Sharma, Suman, C. S. Pundir, N. Sehgal, and A. Kumar, "Galactose sensor based on galactose oxidase immobilized in polyvinyl formal," *Sensors and Actuators B: Chemical*, vol. 119, no. 1, pp. 15–19, 2006.

[21] T. Yao and K. Takashima, "Amperometric biosensor with a composite membrane of sol-gel derived enzyme film and electrochemically generated poly(1,2-diaminobenzene) film," *Biosensors & Bioelectronics*, vol. 13, no. 1, pp. 67–73, 1998.

[22] E. Ekinci and A. Paşahan, "Poly (4-methoxyphenol) film as a galactose-sensing material," *European Polymer Journal*, vol. 40, no. 8, pp. 1605–1608, 2004.

[23] S. J. Cho, H. B. Noh, M. S. Won, C. H. Cho, K. B. Kim, and Y. B. Shim, "A selective glucose sensor based on direct oxidation on a bimetal catalyst with a molecular imprinted polymer," *Biosensors & Bioelectronics*, vol. 99, pp. 471–478, 2018.

[24] D. Das, D. M. Kim, D. S. Park, and Y. B. Shim, "A glucose sensor based on an aminophenyl boronic acid bonded conducting polymer," *Electroanalysis*, vol. 23, no. 9, pp. 2036–2041, 2011.

[25] Y. Zhang, M. K. Ram, E. K. Stefanakos, and D. Y. Goswami, "Synthesis, characterization, and applications of ZnO nanowires," *Journal of Nanomaterials*, vol. 2012, Article ID 624520, 22 pages, 2012.

[26] Z. Zhao, W. Lei, X. Zhang, B. Wang, and H. Jiang, "ZnO-based amperometric enzyme biosensors," *Sensors*, vol. 10, no. 2, pp. 1216–1231, 2010.

[27] Z. Yang, X. L. Zong, Z. Ye, B. Zhao, Q. L. Wang, and P. Wang, "The application of complex multiple forklike ZnO nanostructures to rapid and ultrahigh sensitive hydrogen peroxide biosensors," *Biomaterials*, vol. 31, no. 29, pp. 7534–7541, 2010.

[28] Z. Fan and J. G. Lu, "Zinc oxide nanostructures: synthesis and properties," *Journal of Nanoscience and Nanotechnology*, vol. 5, no. 10, pp. 1561–1573, 2005.

[29] R. Ahmad, M. S. Ahn, and Y. B. Hahn, "ZnO nanorods array based field-effect transistor biosensor for phosphate detection,"

Journal of Colloid and Interface Science, vol. 498, pp. 292–297, 2017.

[30] A. Wei, X. W. Sun, J. X. Wang et al., "Enzymatic glucose biosensor based on ZnO nanorod array grown by hydrothermal decomposition," *Applied Physics Letters*, vol. 89, no. 12, p. 123902, 2006.

[31] X. Liu, Q. Hu, Q. Wu, W. Zhang, Z. Fang, and Q. Xie, "Aligned ZnO nanorods: a useful film to fabricate amperometric glucose biosensor," *Colloids and Surfaces B: Biointerfaces*, vol. 74, no. 1, pp. 154–158, 2009.

[32] N. Palomera, M. Balaguera, S. K. Arya et al., "Zinc oxide nanorod films for electrochemical urea biosensor," *Materials Research Society Symposium Proceedings*, vol. 1355, 2011.

[33] S. N. Sarangi, S. Nozaki, and S. N. Sahu, "ZnO nanorod-based non-enzymatic optical glucose biosensor," *Journal of Biomedical Nanotechnology*, vol. 11, no. 6, pp. 988–996, 2015.

[34] E. Arca, K. Fleischer, and I. V. Shvets, "Influence of the precursors and chemical composition of the solution on the properties of ZnO thin films grown by spray pyrolysis," *Journal of Physical Chemistry C*, vol. 113, no. 50, pp. 21074–21081, 2009.

[35] R. Hong, T. Pan, J. Qian, and H. Li, "Synthesis and surface modification of ZnO nanoparticles," *Chemical Engineering Journal*, vol. 119, no. 2-3, pp. 71–81, 2006.

[36] J.-J. Dong, C. Y. Zhen, H. Y. Hao et al., "Controllable synthesis of ZnO nanostructures on the Si substrate by a hydrothermal route," *Nanoscale Research Letters*, vol. 8, no. 1, p. 378, 2013.

[37] C. V. Sapan, R. L. Lundblad, and N. C. Price, "Colorimetric protein assay techniques," *Biotechnology and Applied Biochemistry*, vol. 29, no. 2, pp. 99–108, 1999.

[38] D. A. Armbruster and T. Pry, "Limit of blank, limit of detection and limit of quantitation," *The Clinical Biochemist Reviews*, vol. 29, article S49, Supplement 1, 2008.

[39] G. L. Long and J. D. Winefordner, "Limit of detection a closer look at the IUPAC definition," *Analytical Chemistry*, vol. 55, no. 7, pp. 712A–724A, 1983.

[40] X. Duan, Y. Li, N. K. Rajan, D. A. Routenberg, Y. Modis, and M. A. Reed, "Quantification of the affinities and kinetics of protein interactions using silicon nanowire biosensors," *Nature Nanotechnology*, vol. 7, no. 6, pp. 401–407, 2012.

The Scientific
World Journal

Journal of
Applied Chemistry

Journal of
Nanomaterials

Scientifica

International Journal of
Polymer Science

Advances in
Chemistry

Advances in
Physical Chemistry

International Journal of
Analytical Chemistry

![Hindawi]

Submit your manuscripts at
www.hindawi.com

Advances in
Condensed Matter Physics

Journal of
Chemistry

International Journal of
Biomaterials

Advances in
High Energy Physics

Journal of
Engineering

Journal of
Nanotechnology

International Journal of
Corrosion

Journal of
Materials

BioMed
Research International

Advances in
Tribology

Advances in
Materials Science and Engineering